# Estimation of residual stresses in laminated composites using field measurements on a cracked sample

Gilles Lubineau


# Estimation of residual stresses in laminated composites using field measurements on a cracked sample

Gilles Lubineau

PII: S0266-3538(08)00229-7
DOI: 10.1016/j.compscitech.2008.06.009
Reference: CSTE 4098

To appear in: *Composites Science and Technology Composites Science and Technology*

Received Date: 13 December 2007
Revised Date: 11 April 2008
Accepted Date: 1 June 2008

Please cite this article as: Lubineau, G., Estimation of residual stresses in laminated composites using field measurements on a cracked sample, *Composites Science and Technology Composites Science and Technology* (2008), doi: 10.1016/j.compscitech.2008.06.009

Gilles Lubineau

*LMT-Cachan (E.N.S. de Cachan / Université Paris 6 / C.N.R.S.)*

*61 Avenue du Président Wilson / 94235 Cachan Cedex, FRANCE*

*Tel : (+33) (0) 147 402 236 / Fax : (+33) (0) 147 402 785*

# Estimation of residual stresses in laminated composites using field measurements on a cracked sample

**Abstract**

**Abstract:** Today, advanced damage models taking into account residual stresses are available. In particular, microcracking as a degradation mechanism in laminates is very sensitive to manufacturing-induced stresses. However, these stresses are often introduced through a model parameter whose identification remains difficult or requires time-consuming and costly additional tests. Here, we propose a relatively simple method based on the observation of the displacement field associated with the creation of a transverse crack in a crosswise laminate. Subsequently, this displacement field can be reinterpreted according to the model being used in order to build the quantity required by the model.

**Keywords:** A - Laminate / C - Residual stress / C - Transverse cracking / D - Optical microscopy

## 1 Introduction

Because of their manufacturing process, laminated composites are subject to residual stresses which can be significant and lead to various consequences between the manufacturing stage and the end of the application's life [1]. These residual stresses can have different sources: thermomechanical sources (different expansion coefficients for the reinforcement and the matrix), chemical sources (matrix shrinkage during polymerization) ... (a review can be found in [2]).

A well-known consequence of these initial residual stresses is the problem of the dimensional stability of molded pieces [3]. As far as mechanical degradation models are concerned, these stresses were long ignored, but today most approaches take them into account in behavior prediction. A classical example, which is reported here, is transverse cracking, a degradation mechanism which is well-documented in the literature (see [4] [5] for reviews). Several authors pinpointed the need to take into account the residual stresses associated with the manufacturing process in estimating the fracture criterion [6] [7] [8]. However, even when the models do manage to integrate these residual stresses, these parameters often remain difficult to identify and evaluate precisely.

A first approach to the resolution of this problem consists in simulating the process as exhaustively as possible in order to deduce these residual stresses from the simulation ([9] [10] ...). This is probably the best solution for the long-term future. Today, however, the number of parameters and physical phenomena involved is too large for the whole evaluation to be controlled. A second solution consists in evaluating these residual stresses within the structure. Thus, a series of destructive or non-destructive experimental approaches was gradually derived for this purpose [11]. A classical estimation technique

*Email address:* lubineau@lmt.ens-cachan.fr (Gilles Lubineau).

consists in observing the effects of these residual stresses on a geometric modification of the structure. Among other works along these lines, one could mention, for example, studies on bimetallic strips [12] or applications of what is known as the "incremental hole" method [13] [14] [15] [16] [17]. Each of these tests must be carried out carefully and represents an additional experiment in the series needed to identify a material.

Here, we propose a simple approach in order to obtain a first approximation of the residual stress state within a ply's material in the context of a study of transverse microcracking. The method consists in observing (using a numerical camera) then analyzing the displacement field generated by the opening of a transverse crack. The multicracking test is classically used in micromechanics to observe crack density/load ratios in order to identify the associated material model [18] [19] [20]. During such a test, each occurrence of a transverse crack results in a localized perturbation of the energy density in its vicinity. The displacement field associated with this perturbation can be calculated through the resolution of a residual problem which can take seemingly different, but actually very similar, forms depending on the authors [4] [21] [22]. Under linear elasticity assumptions, this perturbation is proportional to the residual field which existed along the crack's lip prior to its occurrence. Therefore, by observing this field one can gain some information about the internal stress state of the composite material [23].

In the first section, we review the reference problem, which is about the occurrence of a transverse crack in an initially crack-free crosswise laminate. Through a classical decomposition by superposition, we pinpoint the respective roles of the mechanical loading and the initial residual loading in each component of the field. We also emphasize in the related appendix some properties of the residual field thus introduced.

The second section describes the measurement method itself. The objective is to measure the displacements caused by initial residual stresses. The construction of these displacements requires the comparison of two fields, one obtained experimentally through image analysis, the other obtained numerically through finite element simulation. The experi-

mental method for the construction of the first field is described in details and illustrated in the case of a carbon/epoxy laminate with $[0/90]_s$ lay-up.

In the third section, these residual displacements are interpreted in terms of residual stresses and used to measure the "equivalent polymerization temperature" referred to by several microcracking models [24]. The value obtained is fully consistent with the usually accepted orders of magnitude.

## 2 The reference problem

Let us consider the general case of a cracked cross-ply laminate under generalized plane strains. A more detailed description of the problem is given in Appendix A. Here, we are considering only the two states (cracked and uncracked) of the laminate described in Figure 1.

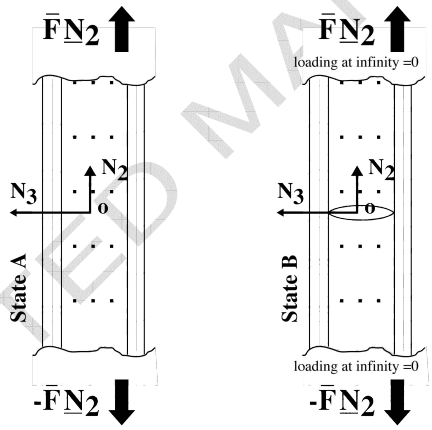


Fig. 1. Cross-ply laminate in traction (A being the healthy state, B the cracked state)

By simple superposition, the field of the displacement jump $\Delta\underline{\mathbf{U}}$ between State A and State B is the result of the combination of the external mechanical loading and the internal residual stresses. Let us simply write:

$$\Delta\underline{\mathbf{U}} = \lambda\underline{\bar{\mathbf{A}}}\bar{F} + \underline{\mathbf{U}}^R \tag{1}$$

where $\bar{F}$ is the external loading, $\lambda\underline{\bar{\mathbf{A}}}$ a linear operator (see Appendix A) and $\underline{\mathbf{U}}^R$ the part of the displacement field associated with the relaxation of the residual stresses over the crack's lips. Here, the objective is to evaluate the residual field $\underline{\mathbf{U}}^R$ to obtain the residual stresses; therefore, we simply transform this equation into:

$$\underline{\mathbf{U}}^R = \Delta\underline{\mathbf{U}} - \lambda\underline{\bar{\mathbf{A}}}\bar{F} \tag{2}$$

Equation 2 involves the mechanical loading (Part $[\lambda\underline{\bar{\mathbf{A}}}\bar{F}]$), the observed displacement fields (Part $[\Delta\underline{\mathbf{U}}]$) and the displacements associated with the residual stresses (Part $[\underline{\mathbf{U}}^R]$). Thus, we are going to use this relation to recover the field $\underline{\mathbf{U}}^R$ associated with the initial residual stresses.

## 3 Estimation of the residual displacement $\underline{\mathbf{U}}^R$

Thus, the construction of the residual displacement field $\underline{\mathbf{U}}^R$ from Equation 2 requires / an experimental field: $\Delta\underline{\mathbf{U}}$ / and a numerical field: $\lambda\underline{\bar{\mathbf{A}}}\bar{F}$.

Here, we will illustrate the method in the case of a crosswise laminate consisting of a $[0/90]_s$ lay-up of width b=20mm. The elementary ply has a width of 0.142mm and its material characteristics are given in Table 1.

| $E_{ll}$ $(MPa)$ | $E_{tt}$ $(MPa)$ | $\nu_{lt}$ | $\nu_{tt}$ | $G_{lt}$ (MPa) |
|---|---|---|---|---|
| 157,000 | 8,500 | 0.29 | 0.4 | 5,000 |

Table 1

Elastic properties of the carbon-epoxy material being used

The material is an IM7/977-2 carbon-epoxy provided by EADS, which was in charge of optimizing the polymerization cycle for a supersonic application (a completely stable polymerized material free from post-baking effects). In order to achieve a minimal residual

polymerization rate, a post-baking cycle was added to the customary cycle used for this material in subsonic applications. The cycle chosen consisted of a 3-hour gelation phase at 150°c followed by a 2-hour polymerization phase at 180°C. Cooling and heating were applied at a rate of 2°C/mn. A pressure of 7 bars was applied from the beginning of the cycle until the return to ambient temperature. Post-baking consisted of heating at a rate of 3°C/mn until 210°C, followed by 2 hours at constant 210°C temperature, then cooling at a rate of 3°C/mn until the return to ambient temperature.

### *3.1 Measurement of Field* $\Delta\underline{\mathbf{U}}$

This measurement was carried out based on an observation of the sample area using a numerical camera. A numerical camera mounted on a long-distance QUESTAR microscope (Figure 2) enabled us to acquire data on the edge of the sample.

The macroscopic loading was incremented in $\Delta F$ steps. For each load level ($F_n = n\Delta F$), a series of pictures was taken through automatic scanning of the sample area. (This step was required because the position of the future crack was of course unknown.) The procedure was repeated for each increment. When a transverse crack was detected, the load level was reduced down to the previously recorded level. Then, a picture of the cracked zone was taken in order to play the role of Picture B.

Thus, we had pictures of the zone before and after cracking (Figure 3) corresponding to the same load level ($F_A = F_B = F$). The size of both pictures was $1024 * 1280 px^2$. The resolution was 1.66 pixel/micron.

Next, the field of the displacement vectors $\Delta\underline{\mathbf{U}}^{A\to B}$ between the two pictures A and B was obtained by image analysis. The classical technique [25] [26] consists in dividing the zone of interest of Picture A (hereafter denoted $S_{Obs}$) into elementary patterns following a regular grid (Figure 4). Then, each elementary zone of Picture A is sought in Picture B by correlation, leading to the displacement of the center of the elementary pattern. Thus,

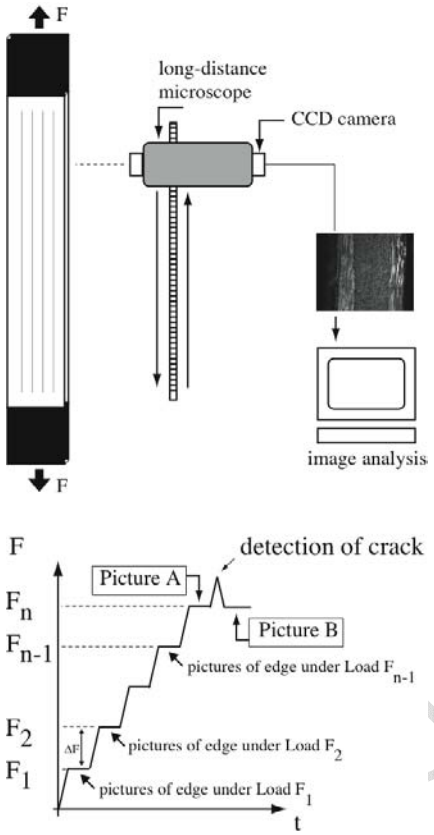


Fig. 2. Setup for the optical observation and incremental scanning of the edge of the crosswise laminate

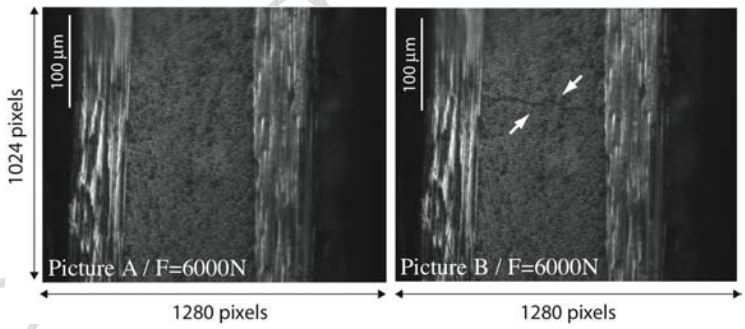


Fig. 3. Pictures of the zone of interest before and after cracking

the displacement field $\Delta\underline{\mathbf{U}}^{A\to B}$ is obtained in discrete manner at the center of each of the elementary zones. In our case, this operation was carried out using the code CORRELIQ2, which uses a more elaborate version of this technique in which the relative displacements are interpolated through a finite-element approximation [27]. This is illustrated in Figure 5[b], which shows $\Delta\mathbf{U}^{2^{A\to B}}$ (the displacement field according to $\underline{N}_2$ between the two

pictures) expressed in pixels in the $[Q; \underline{N}_2, \underline{N}_3]$ coordinate system.

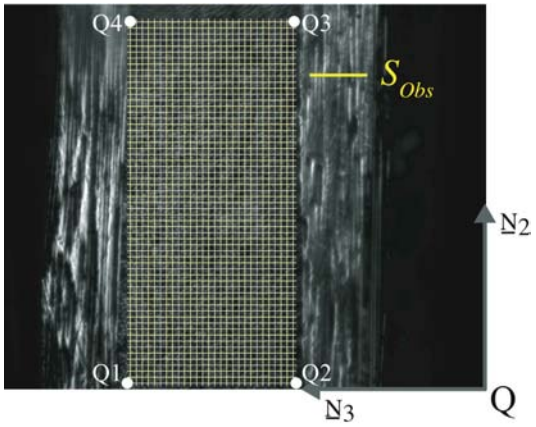


Fig. 4. The zone of interest $S_{Obs}$ and the decomposition grid of the reference picture for image analysis purposes

This is the raw information issued from the analysis. In order to obtain usable information, two additional operations were carried out on the measured field:

**filtering:** The raw field obtained in Figure 5 [b] is highly perturbed. The greater part of this perturbation comes from the dimension of the observation in relation to that of the fiber/matrix arrangement. Indeed, the elementary zones used were 16*16 pixels. Each elementary zone contained about 2 to 3 fibers, which is less than the representative elementary volume of the homogenized arrangement. Therefore, we carried out some smoothing of the solution (Figure 5[c]), which is equivalent to homogenizing the result, leading to the effective elimination of the perturbation related to the microstructure. Several smoothing techniques were tested and compared. The key characteristics of the smoothing method which was finally chosen are described in Annex B. Obtaining a "clean" field is a prerequisite to an effective suppression of the rigid body movement.

**truncation:** the displacement field in the immediate vicinity of the crack was not taken into account. For one thing, its extraction by image analysis is difficult. Besides, even if this field could be extracted correctly, it would still depend on the local morphology of the crack and would not be a reliable quantity (even though the perturbations due

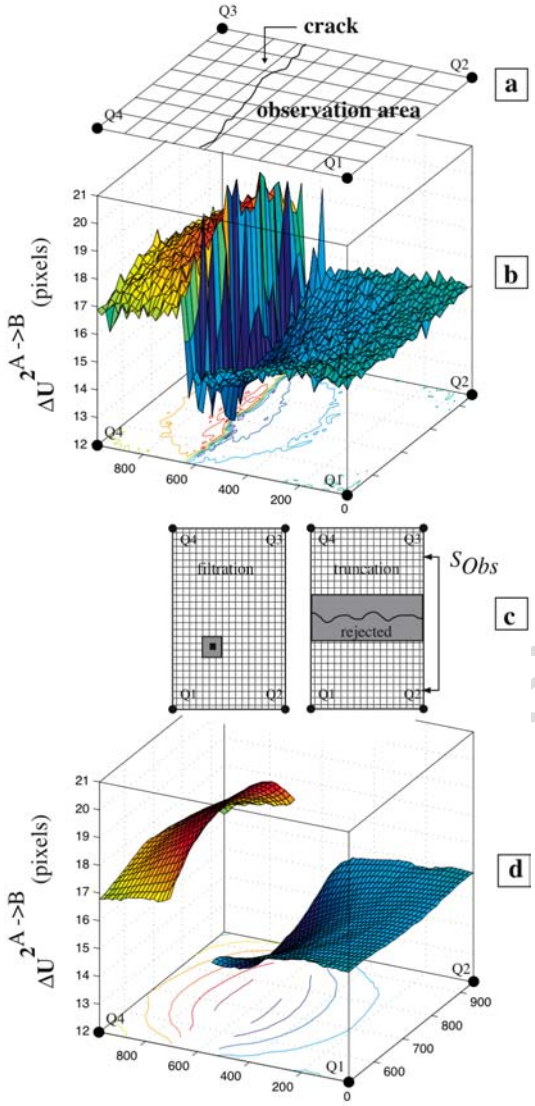


Fig. 5. Processing of the observed displacement field

to the local morphology subside very rapidly, see Annex B). Therefore, it was removed (Figure 5[c]) in order to retain only information which is independent of the local profile of the crack.

Once these two operations carried out, we obtained the informative field of Figure 5[d]. It was relatively easy to remove the rigid-body movement in order to extract the displacement field $\mathbf{\Delta U^2}|_{S_{Obs}}$ expressed in the $[O; \underline{N}_2, \underline{N}_3]$ coordinate system (see appendix C). Finally, the field $\mathbf{\Delta U^2}|_{S_{Obs}}$, which is the restriction of $\mathbf{\Delta U}^2$ to the observed surface

$S_{Obs}$ is illustrated, in microns, in Figure 6.

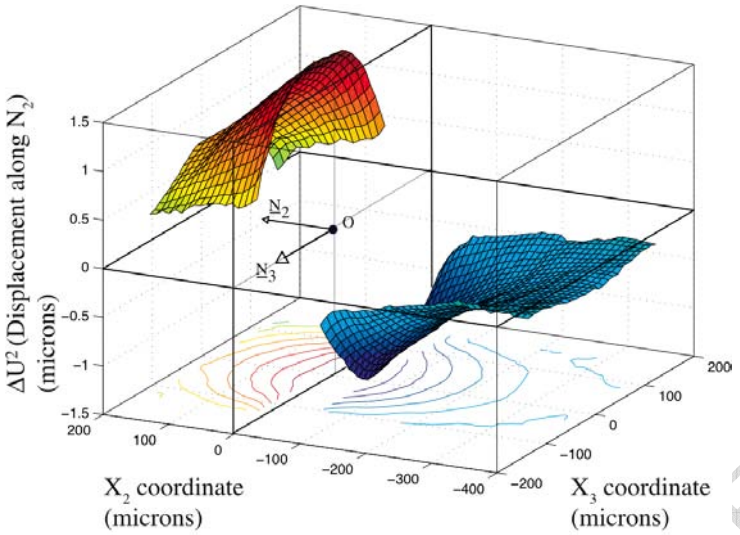


Fig. 6. The displacement field $\Delta\mathbf{U^2}|_{\mathbf{S_{Obs}}}$

Here, the experimental results were illustrated by treating only the component of the displacement field along $\underline{N}_2$. In the rest of this article, we will use this component alone. Of course, the method can also be applied to Component 3 in order to supplement the identification and make it more robust.

### *3.2 Construction of Field* $[\lambda\bar{\underline{\mathbf{A}}}F]$

The operator $\bar{\underline{\mathbf{A}}}$ is obtained simply as the displacement field of the finite element problem described in Figure 7. This is a generalized plane strain problem subjected to a uniform unit residual along the crack's lip with zero loading at infinity. (In practice, a finite problem with length $L > 10H$ provides a good approximation.) This is a problem with natural boundary conditions alone which is slightly different from that described in [28]. Then, the component $\bar{\mathbf{A}}^{\mathbf{2}}$ associated with the displacement in the $\underline{N}_2$ direction is illustrated in Figure 7.

This displacement is shown in Figure 8 for the macroscopic load corresponding to the experimental observation $F = 6,000N$ on the observation zone $S_{Obs}$. This field can now

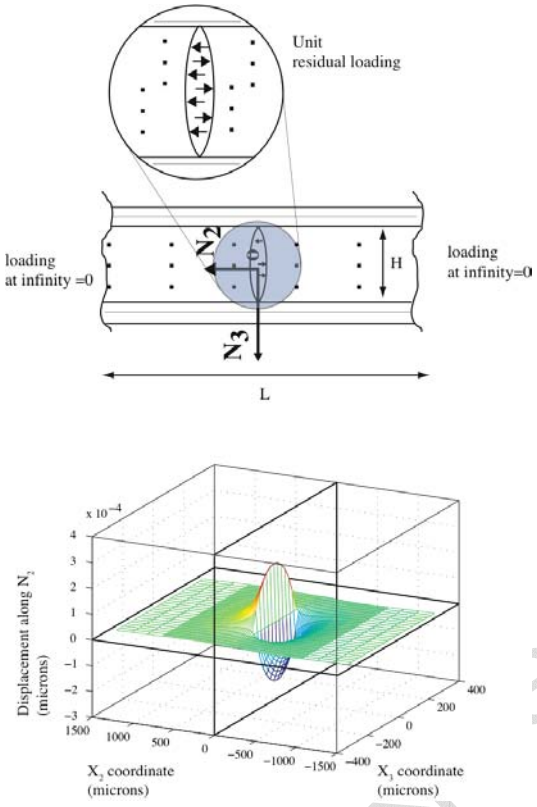


Fig. 7. The FE problem for the determination of Operator $\underline{\bar{\mathbf{A}}}$ and the displacement field $\bar{\mathbf{A}}^{\mathbf{2}}$ associated with a unit macroscopic load

be compared to the experimental field $\Delta\mathbf{U^2}|_{\mathbf{S_{Obs}}}$.

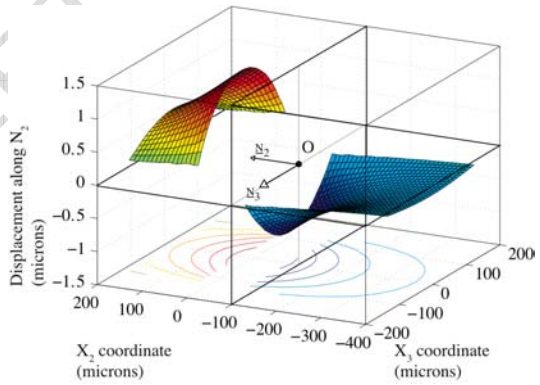


Fig. 8. The displacement field $\lambda\bar{\mathbf{A}}^{\mathbf{2}}\bar{F}$ associated with a macroscopic load $b.\bar{F} = F = 6000N$

### *3.3 Back to the residual field* $\underline{\mathbf{U}}^R$

The comparison of Fields $\Delta\mathbf{U^2}|_{\mathbf{S_{Obs}}}$ and $[\lambda\bar{\mathbf{A}}^{\mathbf{2}}\bar{F}]$ (figure 9) tells us about the magnitude of the initial residual stresses.

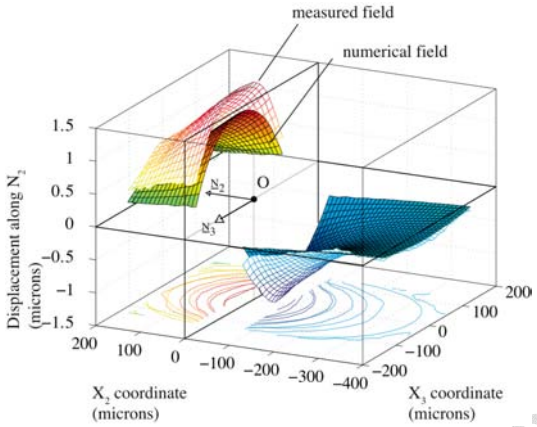


Fig. 9. Superposition of Fields $\Delta\mathbf{U^2}|_{\mathbf{S_{Obs}}}$ and $[\lambda\underline{\bar{\mathbf{A}}}\bar{F}_B]$

Thus, the displacement field $\mathbf{U}^{2R}$ can be estimated. It is shown in Figure 10.

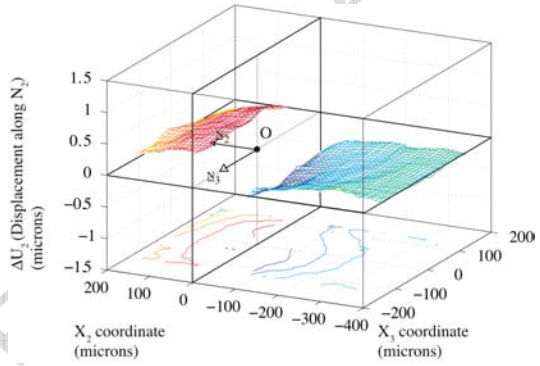


Fig. 10. The residual displacement field $\mathbf{U}^{2R}$

## 4 Estimation of the initial residual stresses

At this point, the interpretation of the residual displacement $\mathbf{U}^{2R}$ in terms of initial stresses requires that a number of assumptions be made. Here, we will consider the most common and simplest case:

- *Assumption H3: the initial stresses are assumed to be uniform across the thickness of the elementary ply* (of course, only through the thickness of the ply of interest; they may vary between plies.)

Under this assumption, the residual field must read:

$$\mathbf{U}^{2R} = \bar{\mathbf{A}}^{\mathbf{2}}\sigma^R \tag{3}$$

Thus, the initial residual stress is obtained by minimizing a distance $D$ between the measured field and the theoretical field. Here, this distance is defined simply by:

$$D(\sigma^R) = \sqrt{\int_{S_{Obs}} \frac{\left(\mathbf{U}^{2R} - \bar{\mathbf{A}}^{\mathbf{2}}\sigma^R\right)^2}{S_{Obs}} dS_{Obs}} \tag{4}$$

Function $D$ is shown in Figure 11. For the measurement which was carried out, we observe an initial residual stress level of about 22MPa, which is fully consistent with classical orders of magnitude.

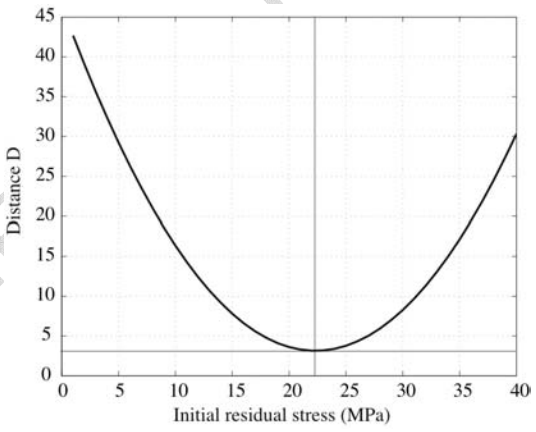


Fig. 11. $D$ as a function of $\sigma^R$

Numerous microcracking models assume the existence of an initial prestress. This prestress is usually calculated as a "thermal prestress" related to a temperature variation $\Delta T$. With a very coarse approximation of the laminate in 1D, one obtains classically

(with $\alpha_l$ and $\alpha_t$ being the expansion coefficients along the fiber and across respectively):

$$\Delta T = \frac{E_{ll} + E_{tt}}{E_{ll} \cdot E_{tt} \cdot (\alpha_l - \alpha_t)} \sigma^R \tag{5}$$

For the material being considered, $\alpha_l \approx 0$ and $\alpha_t \approx 30.10^{-6}$. Thus, in this case, the temperature variation equivalent to the process would be around $-75^oC$, which is in agreement with commonly accepted values. Let us note that the exact interpretation of the quantity obtained here differs from that presented in other approaches, such as in [24]. In the "master plot analysis" type of approach, the determination of the thermal prestress is achieved through a microcracking development model. Therefore, the temperature variation which must be introduced is highly dependent on the cracking model. Thus, in the case of an $AS4/3501-6$, [24] ends up with two different values ($-95^oC$ and $-143^oC$) depending on whether cracking is assumed to occur under prescribed displacement or prescribed load. In our approach, no degradation model is introduced. Cracking is introduced only to create the heterogeneous field necessary to give rise to residual stresses. Therefore, this quantity is common to all subsequent mechanisms. This approach also has the advantage of allowing one measurement point for each transverse crack, which enables dozens of possible evaluations from a single multicracking test.

## 5 Conclusion

In this paper, we propose a method for the estimation of residual stresses based on post-processing a displacement field measured with a numerical camera on a crosswise laminate, then comparing this field with a finite element calculation. This method has the advantages of being relatively simple to implement and using a test already included in classical identification procedures for laminates. The use of a field measurement enables one to make the measurement robust because it is relatively insensitive to the profile of the crack being considered. Of course, this method can be used throughout the multicracking

test and reused at the occurrence of each new crack. This will significantly enhance both the accuracy of the method and its robustness, and will be the subject of forthcoming works.

## A Detailed reference problem

Let us consider a crosswise laminate subjected to a macroscopic solicitation in traction (Figure A.1[a]). Two states are being considered: State A before cracking (with the traction load $F_A$), and State B after cracking (with the traction load $F_B > F_A$).

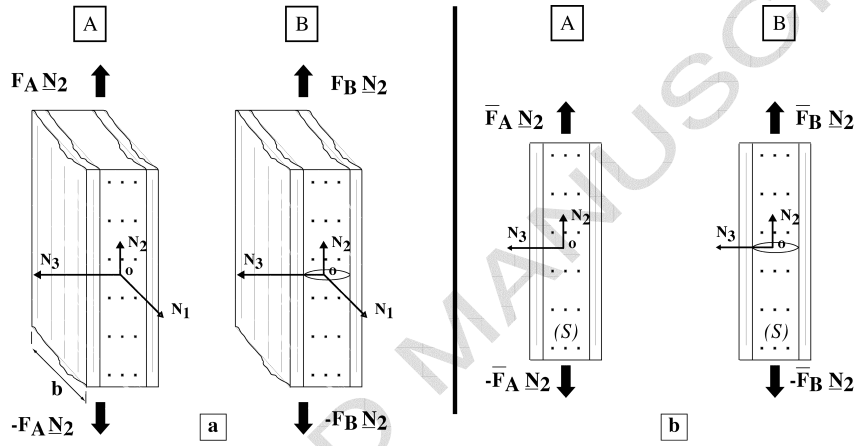


Fig. A.1. [a]: crosswise laminate in traction (A is the healthy state and B the cracked state) [b]: simplified problems in generalized plane strain ($\bar{F} = \frac{F}{b}$)

The whole study will be carried out under the following assumptions:

- *Assumption A1: the problem is independent of the direction* $\underline{N}_1$. This is equivalent both to neglecting the edge problem and to assuming a crack crossing through the ply width. Here, this assumption is legitimate (the edge effect has been verified to be negligible by a FE analysis, and the crossing of the crack has been observed by X-Ray), but this may not always be the case depending on the sequence being used. In that case, the method presented here can still be applied using a 3D finite element reanalysis in order to improve its accuracy. This will be the subject of a forthcoming paper.

- *Assumption A2: the material's behavior is linear elastic.*

*A1* enables us to define simplified problems over a plane domain $S$ (Figure A.1 [b]). These are generalized plane strain problems, and all the displacement fields will be expressed in the coordinate system $[O; \underline{N}_2, \underline{N}_3]$, $O$ being the "center" of the crack. In the following sections, we will consider only the plane part of these displacements.

Remark: a bold quantity $\mathbf{X}$ designates a field over $S$, and an underlined quantity $\underline{X}$ denotes a vector. A quantity both bold and underlined $\underline{\mathbf{X}}$ designates a vector field over $S$. Thus, $\mathbf{X}^i$ is the scalar field associated with the component $i$ of the vector field $\underline{\mathbf{X}}$.

■ **For State A**, the field of the displacement vectors $\underline{\mathbf{U}}^A = [\mathbf{U}^{2^A}\underline{N}_2 + \mathbf{U}^{3^A}\underline{N}_3]$ can be expressed as:

$$\underline{\mathbf{U}}^A = [\tilde{\mathbf{A}}^2\underline{N}_2 + \tilde{\mathbf{A}}^3\underline{N}_3]\bar{F}_A = \underline{\tilde{\mathbf{A}}}\bar{F}_A \tag{A.1}$$

where $\underline{\tilde{\mathbf{A}}}$ is the field of the displacement vectors which corresponds to a unit macroscopic load. In the case of Assumption *A1*, this operator can be easily obtained analytically using the classical theory of laminates.

■ **For state B**, the field of the displacement vectors $\underline{\mathbf{U}}^B$ can be expressed as the superposition of a crack-free solution $\underline{\mathbf{U}}^B_{①}$ and a residual solution $\underline{\mathbf{U}}^B_{②}$ (see Figure A.2):

$$\underline{\mathbf{U}}^B = \underline{\mathbf{U}}^B_{①} + \underline{\mathbf{U}}^B_{②} \tag{A.2}$$

Of course, as far as Solution ① is concerned:

$$\underline{\mathbf{U}}^B_{①} = \underline{\tilde{\mathbf{A}}}\bar{F}_B \tag{A.3}$$

Then, this healthy solution is corrected through the residual problem in order to build the exact solution. Problem ② is linear with respect to the residual loading onto the crack's lip, denoted $P$.

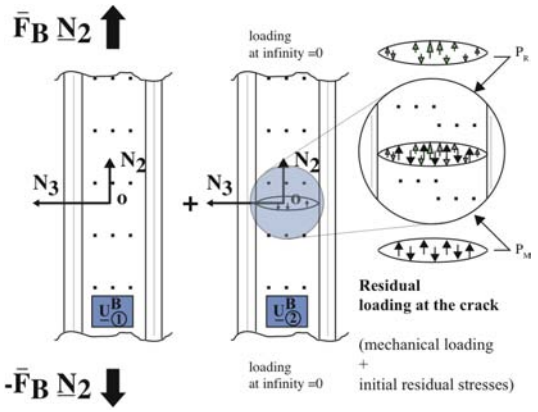


Fig. A.2. Decomposition of State B into a healthy solution and a residual solution

□ In the absence of residual internal stresses, $P$ consists only of a part associated with the mechanical loading $\bar{F}_B$, denoted $P_M$. Of course, $P_M$ is proportional to $\bar{F}_B$ with a known proportionality coefficient denoted $\lambda$. Thus, in that case:

$$P = P_M = \lambda \bar{F}_B \tag{A.4}$$

The crack also introduces a residual displacement field of the form:

$$\underline{\mathbf{U}}^B_{②} = [\bar{\mathbf{A}}^2 \underline{N}_2 + \bar{\mathbf{A}}^3 \underline{N}_3] P = \lambda \underline{\bar{\mathbf{A}}} \bar{F}_B \tag{A.5}$$

where $\underline{\bar{\mathbf{A}}}$ is the field of the displacement vectors associated with a unit residual and uniform over the crack's lip.

□ In the presence of internal residual stresses $P_R$, the residual $P$ becomes:

$$P = P_M + P_R \tag{A.6}$$

$P_R$ is *a priori* not necessarily uniform over the cracked surface. Therefore, in general, the displacement of the residual problem ② can be written as:

$$\underline{\mathbf{U}}^B_{②} = \lambda \underline{\bar{\mathbf{A}}} \bar{F}_B + \underline{\mathbf{U}}^R \tag{A.7}$$

$\underline{\mathbf{U}}^R$ is the part of the displacement field associated with the relaxation of the residual stress over the crack's lip. The objective of the rest of this paper is to measure, then

interpret this quantity in order to gather information on the existing residual stresses. By combining A.3 and A.7, one can express the field of the displacement vectors in Configuration B:

$$\underline{\mathbf{U}}^B = \underline{\tilde{\mathbf{A}}}\bar{F}_B + \lambda\underline{\bar{\mathbf{A}}}\bar{F}_B + \underline{\mathbf{U}}^R \tag{A.8}$$

Let $\Delta\underline{\mathbf{U}} = \underline{\mathbf{U}}^B - \underline{\mathbf{U}}^A$ be the field of the displacement jump vectors between State A and State B. From A.1 and A.8, one has:

$$\underline{\mathbf{U}}^R = \Delta\underline{\mathbf{U}} - \underline{\tilde{\mathbf{A}}}(\bar{F}_B - \bar{F}_A) - \lambda\underline{\bar{\mathbf{A}}}F_B \tag{A.9}$$

Now, assuming that $\bar{F}_B = \bar{F}_A = \bar{F}$, Equation A.9 reduces to:

$$\underline{\mathbf{U}}^R = \Delta\underline{\mathbf{U}} - \lambda\underline{\bar{\mathbf{A}}}\bar{F}_B \tag{A.10}$$

## B Smoothing and truncation

The solution chosen is based on an interpolation of the measured field in the vicinity of each point $\underline{M}$. One defines the plane $\Pi_{\underline{M}}$ which provides the best fit, in the least-squares sense, to the displacement field in the vicinity of $\mathcal{V}(\underline{M})$. Then, the "smoothed" value of the displacement field at Point $\underline{M}$ is defined as $\Pi_{\underline{M}}[\underline{M}]$ (Figure B.1).

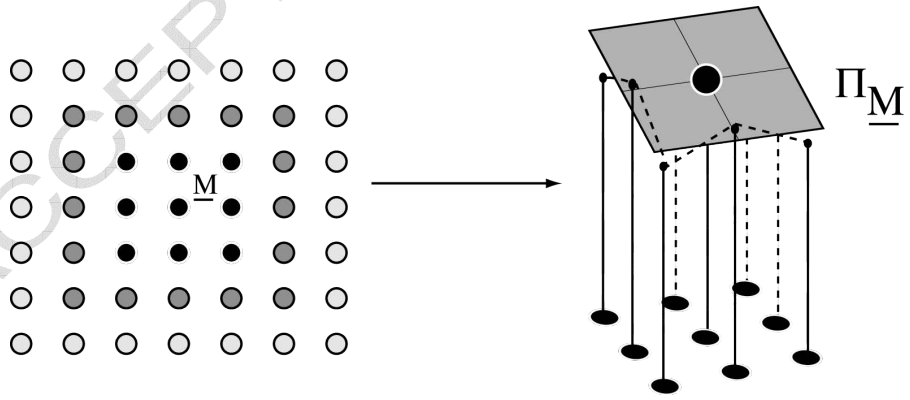


Fig. B.1. Vicinity and approximation plane for the smoothing procedure

For a square smoothing zone, let $(2L+1)^2$ denote the number of points taken into account

in the vicinity. Various levels of smoothing (L=1, L=2, L=3) were tested and no significant difference was found (Figure B.2). $L = 2$ was chosen for all the plots.

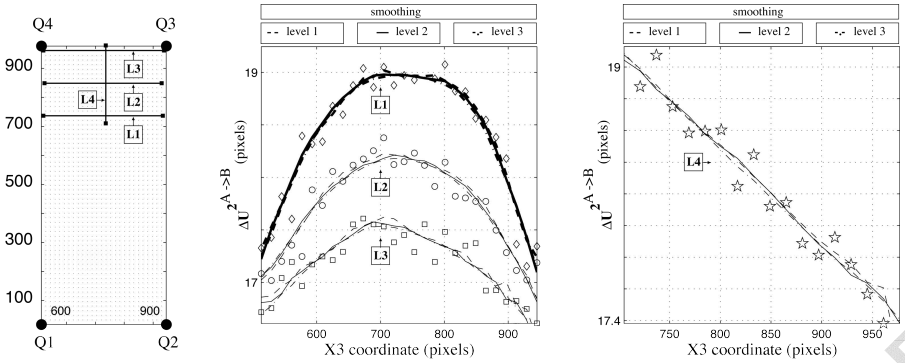


Fig. B.2. Comparison of the measured and smoothed fields over different characteristic lines. The dots correspond to direct measurements and the lines to progressive approximation levels

Regarding truncation, this operation was performed to remove perturbations inherent in the geometrical defects of the crack's lip. A rapid finite element analysis (see Figure B.3) showed that the perturbations due to the cracks' local profile subside very quickly, which confirms the advantage of a field measurement compared to a local measurement of the lip's opening.

Thus, in practice, the size of the exclusion zone is guided mainly by constraints related to the field measurements. If the interpolation zones are $Npx * Npx$ pixels, this exclusion zone must obviously be at least $Npx + L_c$ pixels wide, $L_c$ being the width of the crack generated by its waviness. In the example given here, $Npx = 16px$ and $L_c \approx 60px$. The minimum size of the exclusion zone is about $80px$. In practice, we recommend a size of the order of the ply's thickness.

## C Suppression of the rigid body mode

The measured field $\Delta\mathbf{U^2}|_{S_{Obs}}$ is the superposition of a residual field of interest $\Delta\mathbf{U^{2r}}|_{S_{Obs}}$ and a rigid body field (due, for example, to the variation in the stiffness of the sample

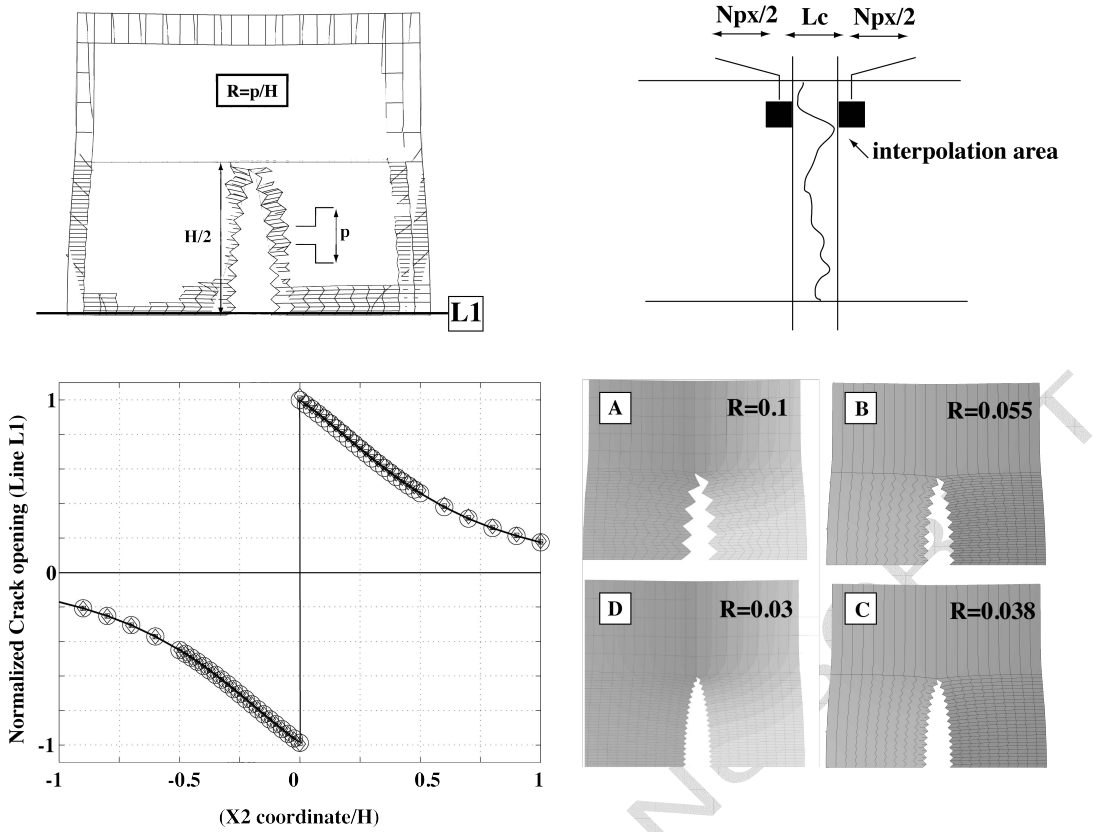


Fig. B.3. Comparison of the residual displacements for lips with varying roughness

caused by the crack, a poor repositioning of the camera between shots A and B, small differences in macroscopic loads between shots,...). Here, first of all, we give the key steps to suppress this rigid body mode when it reduces to a pure translation along $\underline{N}_2$. In order to simplify, let us consider the diagram of Figure C.1 [a], representing the displacement field $\Delta\mathbf{U^2}|_{S_{Obs}}$ (here, again for the sake of simplicity, a curve with normal $\underline{N}_3$). The residual part is generated by an ideal "virtual" crack whose abscissa is, of course, unknown, but bounded by $X^-$ and $X^+$. Let $X_2^{ref}$ denote the abscissa of the theoretical crack chosen between $X^-$ and $X^+$.

- **Step 1:** Choose an arbitrary value of $X_2^{ref}$
- **Step 2:** Express the displacement in a coordinate system centered on this new virtual crack. In 1D, this consists in defining a new field $\Delta\mathbf{U^2}|_{S_{Obs}}^{step1}$ (Figure C.1[b]):

$$\Delta\mathbf{U^2}|_{S_{Obs}}^{step1}(x_2) = \Delta\mathbf{U^2}|_{S_{Obs}}(X_2 = x_2 + X_2^{ref}) \tag{C.1}$$

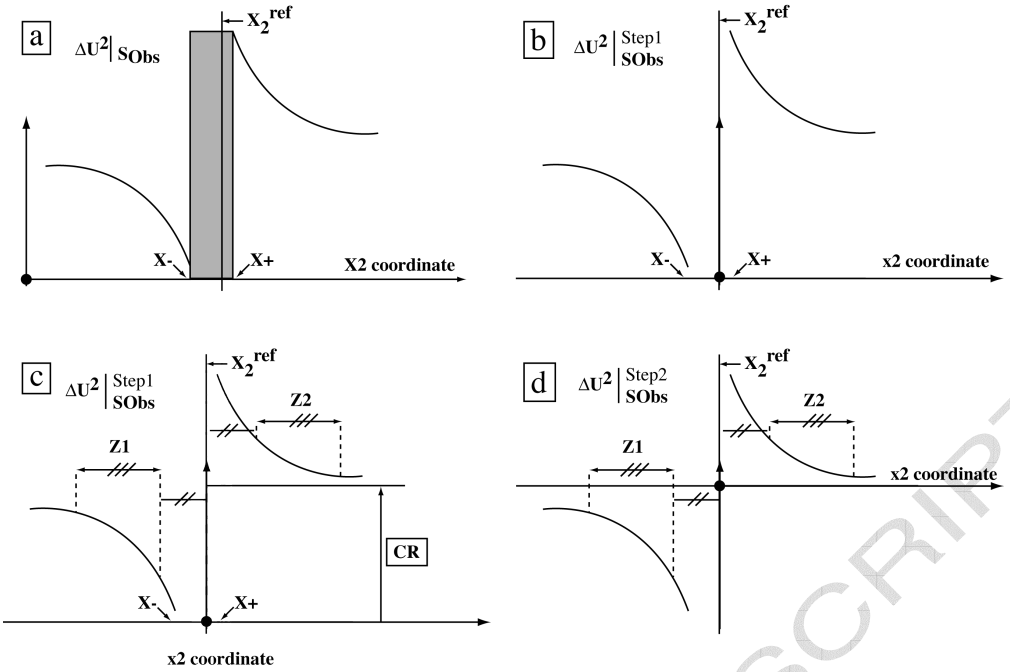


Fig. C.1. Step-by-step construction of the residual field for a predefined position of the "ideal" crack

- **Step 3:** Remove the "rigid body" part for this test; Z1 and Z2 are two symmetrical zones in the new coordinate system, chosen to be as large as possible depending on the available data (Figure C.1[c]):

$$CR = \frac{1}{2} \cdot \int_{Z1 \cup Z2} \left\{ \Delta \mathbf{U^2}|_{S_{Obs}}^{step1}(x) + \Delta \mathbf{U^2}|_{S_{Obs}}^{step1}(-x) \right\} dx \tag{C.2}$$

in order to build the new field $\Delta \mathbf{U^2}|_{S_{Obs}}^{step2}$ (Figure C.1[d]):

$$\Delta \mathbf{U^2}|_{S_{Obs}}^{step2}(x_2) = \Delta \mathbf{U^2}|_{S_{Obs}}^{step1}(x_2) - CR \tag{C.3}$$

- **Step 4:** Define a quality indicator for the reconstructed solution, in the form:

$$QUAL = \frac{1}{2} \cdot \int_{Z1 \cup Z2} \left| \Delta \mathbf{U^2}|_{S_{Obs}}^{step2}(x) + \Delta \mathbf{U^2}|_{S_{Obs}}^{step2}(-x) \right| dx \tag{C.4}$$

The quality indicator is minimum (theoretically zero in the case of perfect measurements) when $X_2^{ref}$ corresponds to the position sought for the virtual crack. The whole approach relies on the fact that the exact residual field is skew-symmetric with respect to $x_2$.

Thus, this procedure enables one both to determine effectively the underlying "perfect" crack (which is needed for comparison with the subsequent finite element analysis) and to remove the rigid body mode very precisely. The extension to the case of a general in-plane rigid body mode (two translations and one rotation) is straightforward.

## References


[1] P. P. Parlevliet, H. E. N. Bersee, A. Beukers, Residual stresses in thermoplastic composites - a study of the literature. part iii: Effects of thermal residual stresses, Composites Part A: Applied Science and Manufacturing 38 (6) (2007) 1581–1596.

[2] P. P. Parlevliet, H. E. N. Bersee, A. Beukers, Residual stresses in thermoplastic composites–a study of the literature–part i: Formation of residual stresses, Composites Part A: Applied Science and Manufacturing 37 (11) (2006) 1847–1857.

[3] C. K. Huang, S. Y. Yang, Warping in advanced composite tools with varying angles and radii, Composites Part A: Applied Science and Manufacturing 28 (9-10) (1997) 891–893.

[4] J.-M. Berthelot, Transverse cracking and delamination in cross-ply glass-fiber and carbon-fiber reinforced plastic laminates: Static and fatigue loading, Appl. Mech. Rev. 56 (2003) 111–147.

[5] J. Nairn, S. Hu, Matrix microcracking, in: Taljera (Ed.), Damage Mechanics of Composite Materials, 1994, pp. 187–243.

[6] J. A. Nairn, Fracture mechanics of composites with residual thermal stresses, J. Appl. Mech. 64 (1997) 804–810.

[7] D. Perreux, D. Lazuardi, The effects of residual stress on the non-linear behaviour of composite laminates part i. experimental results and residual-stress assessments, Composites Science and Technology 61 (2) (2001) 167–175.

[8] D. Perreux, D. Lazuardi, The effect of residual stress on the non-linear behaviour of composite laminates part ii. layer, laminate non-linear models and the effect of residual stress on the model parameters, Composites Science and Technology 61 (2) (2001) 177–190.

[9] G. Fernlund, A. Osooly, A. Poursartip, R. Vaziri, R. Courdji, K. Nelson, P. George, L. Hendrickson, J. Griffith, Finite element based prediction of process-induced deformation of autoclaved composite structures using 2d process analysis and 3d structural analysis, Composite Structures 62 (2) (2003) 223–234.

[10] E. Ruiz, F. Trochu, Numerical analysis of cure temperature and internal stresses in thin and thick rtm parts, Composites Part A: Applied Science and Manufacturing 36 (6) 806–826.

[11] P. P. Parlevliet, H. E. N. Bersee, A. Beukers, Residual stresses in thermoplastic composites–a study of the literature–part ii: Experimental techniques, Composites Part A: Applied Science and Manufacturing 38 (3) (2007) 651–665.

[12] W. J. Jun, C. S. Hong, Effect of residual shear strain on the cured shape of unsymmetric cross-ply thin laminates, Composites Science and Technology 38 (1) (1990) 55–67.

[13] I. Zhandanov, A. Gonchar, Determining the residual welding stresses at depth in metals, Automatic Welding 31 (1978) 22–4.

[14] E. Beaney, Measurement of sib-surface stress, CEGB Report Rd/B/N4325 .

[15] M. Bateman, O. Miller, T. Palmer, C. Breen, E. Kingston, D. Smith, M. Pavier, Measurement of residual stress in thick section composite laminates using the deep-hole method, International Journal of Mechanical Sciences 47 (11) (2005) 1718–1739.

[16] A. Baldi, Full field methods and residual stress analysis in orthotropic material. i linear approach, International Journal of Solids and Structures 44 (25-26) (2007) 8229–8243.

[17] A. Baldi, Full field methods and residual stress analysis in orthotropic material. ii: Nonlinear approach, International Journal of Solids and Structures 44 (25-26) (2007) 8244–8258.

[18] J. Hoover, D. Kujawski, F. Ellyin, Transverse cracking of symmetric and unsymmetric glass-fibre/epoxy-resin laminates, Composites Science and Technology 57 (1997) 1513–1526.

[19] F. Crossman, A. Wang, The dependence of transverse cracking and delamination on ply thickness in graphite/epoxy laminates, in: K. Reifsnider (Ed.), Damage in composite materials, ASTM-STP 775, 1982, pp. 118–139.

[20] A. Highsmith, K. Reifsnider, Stiffness reduction mechanism in composite laminates, in: K. Reifsnider (Ed.), Damage in Composite Materials, ASTM-STP 775, 1982, pp. 103–117.

[21] Z. Hashin, Analysis of cracked laminates: a variational approach, Mechanical of Materials 4 (2) (1985) 121–136.

[22] J. Nairn, The strain energy release rate of composite microcracking: a variational approach., Journal of Composite Materials 23 (1989) 1106–1129.

[23] N. Takeda, S. Ogihara, Micromechanical characterization of local deformation in interlaminar-toughened cfrp laminates, Composites Part A: Applied Science and Manufacturing 29 (12) (1998) 1545–1552.

[24] J. A. Nairn, Applications of finite fracture mechanics for predicting fracture events in composites, in: Proc. 5th Int'l Conf. on Def. and Fract. of Comp. Mat., London, UK, 1999, p. 1.

[25] M. Sutton, W. Wolters, W. Peters, W. Ranson, S. McNeill, Determination of displacements using an improved digital correlation method, Image and Vision Computing 1 (3) (1983) 133–139.

[26] M. Sutton, C. Mingqi, W. Peters, Y. Chao, S. McNeill, Application of an optimized digital correlation method to planar deformation analysis, Image and Vision Computing 4 (3) (1986) 143–150.

[27] G. Besnard, F. Hild, S. Roux, "finite-element" displacement fields analysis from digital images: Application to portevin-le châtelier bands., Exp. Mech. (46) (2006) 789–803.

[28] P. Ladevèze, G. Lubineau, On a damage mesomodel for laminates: micro-meso relationships, possibilities and limits., Composites Science and Technology 61 (15) (2001) 2149–2158.